Gain and threshold current density characteristics of 2 micron GaInAsSb/AlGaAsSb MQW lasers with increased valence band offset

T. C. Newell, L. F. Lester, X. Wu, Y. Zhang, and A. L. Gray[b]

University of New Mexico
Center for High Technology Materials
1313 Goddard SE
Albuquerque, NM, 87106

[b]U.S. Army Research Laboratory
2800 Powder Mill Road
Adelphi, MD 20783-1145

ABSTRACT

Compressively strained 2 μm GaInAsSb quantum well lasers with large valence band offsets and broadened waveguides display a record characteristic temperature, T_0=140 °K for a 4-QW laser and a differential efficiency of 0.74 for a pulsed 2-QW device. The T_0 of these antimonide lasers is 65% more than that reported for phosphide-based lasers operating at 2 μm wavelength. A room-temperature threshold current density as low as 173 A/cm^2 has been observed for a 2-QW device and 225 A/cm^2 for the 4-QW laser.

Keywords: Semiconductor quantum well lasers, Gallium antimonide

1. INTRODUCTION

As mid-infrared (1.5-5 μm) semiconductor lasers become increasingly prominent, their combination of high power and small size establishes them as potential sources for many applications. These include communications, laser radar (LADAR), chemical sensing, and infrared countermeasures (IRCM). Presently, direct bandgap laser diodes based on GaInAsSb/AlGaAsSb quantum wells (QWs) are the preferred device in the 1.9-2.7 μm regime.[1–5] These lasers have demonstrated low threshold current density and a reasonable differential efficiency.

However, the GaInAsSb/AlGaAsSb heterojunction lattice-matched to GaSb has a type I band offset over only about half of its compositional extent. Within this range, the alloys that yield bandgap wavelengths greater than or equal 2 μm have a theoretical $Q_c = \Delta E_c/\Delta E_g$ that is close to unity. Though the uncertainty in Q_c is large[6] since there have been very few experiments conducted on the material properties of GaInAsSb/AlGaAsSb QWs. Consequently, hole confinement in the QW active region of laser diodes fabricated from these quaternaries may be very poor.

To circumvent this problem, the valence band offset, ΔE_v, can be improved in comparison to lattice matched materials by biaxial strain in the QW.[4] Yet the small saturated gain recently reported for a single strained $Ga_{0.81}In_{0.19}As_{0.02}Sb_{0.98}$well with an $Al_{0.25}Ga_{0.75}As_{0.02}Sb_{0.98}$ barrier suggests that this material design still suffers from inadequate hole confinement.[7] In this manuscript, gain and threshold current density characteristics of strained $Ga_{0.81}In_{0.19}As_{0.02}Sb_{0.98}$QW lasers that have a larger ΔE_v are described and compared to previously published laser results.

Send correspondence to Tim Newell. E-mail: newell@chtm.unm.edu

SPIE Vol. 3284 • 0277-786X/98/$10.00

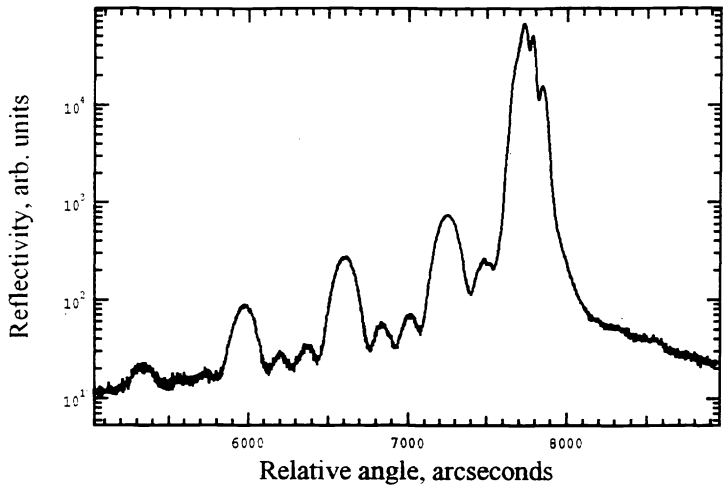

Figure 1. The experimental $\Omega/2\theta$ x-ray diffraction pattern of the GaInAsSb/AlGaAsSb 4-QW structure for the symmetric 004 reflection.

2. MATERIALS GROWTH AND FABRICATION

2- and 4-QW laser structures with 100 $\AA$ $Ga_{0.81}In_{0.19}As_{0.02}Sb_{0.98}$ wells $Al_{0.4}Ga_{0.6}As_{0.03}Sb_{0.97}$ barriers were grown by molecular beam epitaxy (MBE) on a GaSb substrate. These structures employ a broadened waveguide design whereby the core region, composed of the quantum wells, barriers, and separate confinement heterostructure, is 0.922 μm in width. They are similar to those described in Garbuzov[3] except for the following differences: 1) 40% Al in the lattice-matched AlGaAsSb barrier was used for the barrier instead of 25% Al, 2) two 94 $\AA$ QW are employed rather than five 100 $\AA$ QWs, and 3) the core width is slightly different.

Theoretical calculations are based on DeWinter's model[8] to predict the bandgap of GaInAsSb and Landolt-Bornstein[9] along with Tsou[10] for materials data. Computations predict a ΔE_v of 209 meV for the 40% Al in contrast to $\Delta E_v = 140$ meV for a 25% Al barrier. The latter potential normally provides adequate confinement in the GaAs/AlGaAs system. However, it is plausible that a lack of interface abruptness at the GaInAsSb/AlGaAsSb heterojunction causes loss of hole confinement at high current density, even for offsets in the range of 100 meV.

The 4-QW laser structure was analyzed with a Philips double-crystal x-ray diffractometer using the $CuK_{\alpha 1}$ line after 4 symmetric 022 reflections on the surfaces of four Ge crystals (4-crystal Bartels monochromator) and a 0.45-mm receiving slit. X-ray diffractometry profiles of the asymmetric (115) plane and the symmetric (004) plane scans preclude the possibility of strain relaxation in the 4-QW structure. The experimental diffraction profile for the (004) symmetric reflection of the 4-QW laser structure is shown in Fig. 1. The well-defined periodic oscillations are to the left of the substrate peak. These satellite peaks are due to interference between the two Bloch waves in the MQW layers.[11] Their sharpness indicates high-quality, coherently strained wells. Any imperfection, relaxation, or compositional inhomogeneity would cause loss of phase coherence and eliminate the satellite peaks.[12]

Fabry-Perot lasers with 100 μm wide stripes defined by a window in a SiN_x dielectric layer were fabricated on both the 2-QW and 4-QW material. A non-alloyed Ti/Pt/Au ($500\AA/500\AA/2000\AA$) metallization was patterned by the liftoff technique for the ohmic contact to the p-type GaSb cap layer. The wafer was thinned, and the n-type ohmic contact was formed with non-alloyed Pd-Au ($500\AA/2000\AA$). The wafer was cleaved into bars with cavity lengths ranging from 190 μm to 2000 μm. The laser bars were mounted p-side up on a copper heat sink and characterized in pulsed mode.

3. THEORETICAL MODELING

The valence band structure for the $Ga_{0.81}In_{0.19}As_{0.03}Sb_{0.97}/Al_{0.4}Ga_{0.6}As_{0.03}Sb_{0.97}$ quantum well is computed using the $k \cdot p$ method.[13] The procedure begins with the wavefunction, Ψ, which is the solution of $H\Psi = E\Psi$ where the

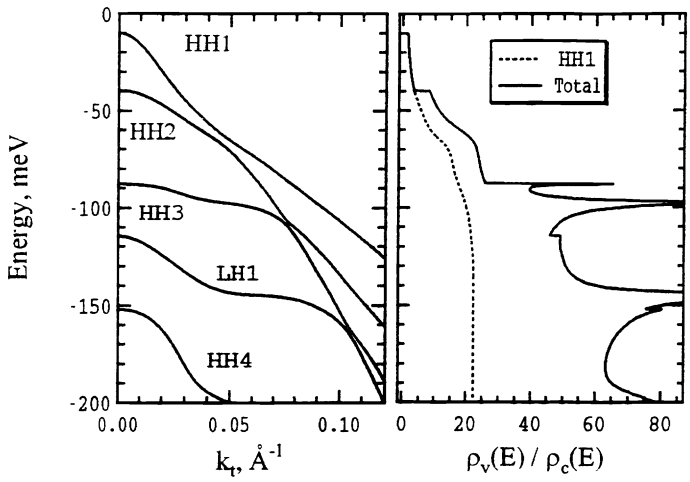

Figure 2. (a) Valence band structure using an average of the [100] and [110] dispersion characteristics. The quantum well depth is $V_o = 209$ meV. The LH1 band is depressed downward in energy due to the material strain. As a result, the HH1 band is nearly parabolic for small values of k_t. (b) The ratio between the valence and conduction bands density of states, $\rho_v(E)/\rho_c(E)$. With little mixing of the HH1 band, the ratio is small for low values of k_t.

Hamiltonian describes transitions between atomic states via dipole interactions.

$$\Psi = \sum_n F_n(r)\,\psi_n(r) \tag{1}$$

where $F(r)$ is the envelope of the Bloch functions, $\psi(r)$. The key role of this second order perturbation method is to provide a means of linking the Bloch function transition matrix elements with experimentally measured effective masses and energy gaps. Then using the envelope function approximation, the remaining problem is solved in terms of the envelope functions.

The original Hamiltonian is the 6x6 Luttinger-Kohn Hamiltonian[14] which is simplified by ignoring the split-off bands. The remaining 4x4 Hamiltonian can be block diagonalized if the direction of the wavevector transverse to the well, k_t, is defined.[15] This leaves a 2x2 matrix in which the diagonal elements represent the heavy, HH, and light hole, LH, bands and the off-diagonal elements gauge the coupling strength. The potential energy terms are just that of a simple finite depth square well. Strain is taken into account via a potential energy correction in the LH matrix diagonal matrix element.[16] The off-diagonal matrix elements are constructed using the average of the 110 and 100 plane wavevector components, which is the axial approximation.[17] The eigenvectors thus represent the HH and LH envelope functions, and the eigenvalues are the energy levels. For the quantum well, the problem is tractable in each barrier and well region. The full solution is obtained by matching wavefunctions at the barrier and well boundaries.

The first four heavy hole bands, HH1..4, along with the first light hole band, LH1, are shown in Fig. 2(a). The effect of strain is to depress the LH1 band so that at $k_t = 0$, $E_{LH1} = -114$ meV. As a result, nearby the band edge the HH1 band only weakly mixes with the other bands and is almost parabolic. Fig. 2(a) also shows regions of large mixing between the HH1 and HH2, HH2 and HH3, and the HH3 and LH1 bands. The consequence of this mixing is strongly manifested in the valence band density of states, $\rho_v(E)$, as seen in the derivative term of the definition, $\rho_v(E) = (k_t/2\pi L)\,(dE/dk_t)^{-1}$. $\rho_v(E)$ is no longer a stairstep function.

Figure 2(b) plots the ratio of $\rho_v(E)$ to the conduction band density of states, $\rho_c(E)$. (Note that in computing $\rho_c(E)$, the conduction bands are considered parabolic.) Near the band edge $\rho_v(E)/\rho_c(E)$ is small. This is due to the absence of strong mixing between the HH1 with the other bands, and it predicts a reduced optical transparency level. At lower energy levels, the plot is significantly altered from the stair step function associated with parabolic

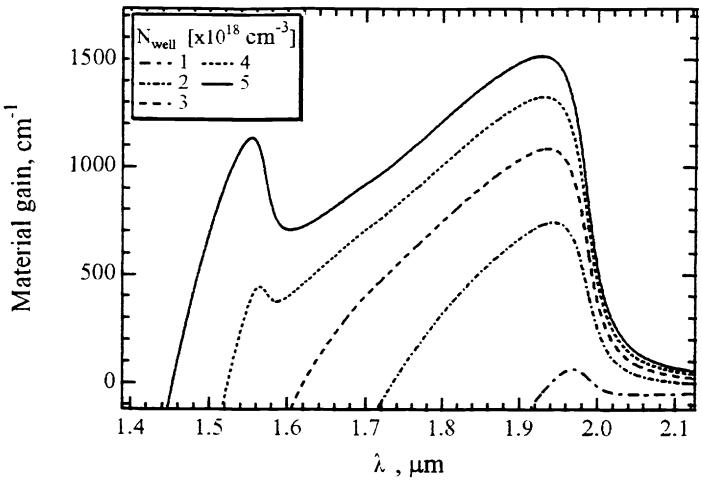

Figure 3. A material gain calculation computed at several values of charge density shows that the CB1-HH1 transition dominates with a peak gain of 1.99 μm. The second peak at 1.57 μm is due to the CB2-HH2 transition. Lorentzian lineshape broadening is incorporated in the calculation.

bands where the step size is a simple measure of the ratio of the electron and hole masses. The spiked regions of large $\rho_v(E)$ / $\rho_c(E)$ are due to flat regions in the particular bands.

Gain calculations for the TE mode are next computed by incorporating the above information, overlap integrals between valence and conduction bands, and calculations of the Fermi levels using

$$g\left(E_{i,j}\right) = |M|^2 \frac{\pi \hbar e^2}{n m_o^2 c \varepsilon_o} \left(\frac{1}{E_{i,j}}\right) \rho_{red}\left(E_{i,j}\right)\left(f_{i,j}^c - f_{i,j}^v\right)\left[I_{i,j}^{e\rightarrow h} + \frac{1}{3} I_{i,j}^{e\rightarrow l}\right] \tag{2}$$

$$g(E) = \sum_{i,j} g\left(E_{i,j}\right) \tag{3}$$

In Eq. 2, $|M|^2$ is the dipole transition matrix element for the valence band Bloch functions, $E_{i,j}$ is the transition energy between conduction, i, and valence, j, bands, ρ_{red} is the reduced density of states [meaning that $\rho_c(E)$ is included in the computation along with $\rho_v(E)$], $f_{i,j}^{c,v}$ is the Fermi occupation probabilities for the conduction and valence bands, and $I_{i,j}$ are the overlap integrals squared between the electron-heavy hole and electron-light hole eigenvectors for the TE mode at the transition energy. The total gain, Eq. 3, is the summation over all transitions. Lineshape broadening is incorporated by convoluting Eq. 3, with a Lorentzian approximation (relaxation time of 0.1 ps). Figure 3 plots the material gain as a function of the emission wavelength for several values of carrier densities within the well. The gain maximum without the convolution integration is 1.99 μm corresponding to the CB1-HH1 transition. For low carrier densities, the other transitions are small and tend to act as loss mechanisms reducing the gain. However, as the carrier density is increased, gain from the CB2-HH2 transition at 1.57 μm increases dramatically compared with the CB1-HH1 transition. Gain due to the CB1-HH1 transition is saturating since the difference in the conduction, f_c, and valence, f_v, band occupation probabilities is approaching unity while this difference in the CB2-HH2 transition is increasing relatively rapidly. Additionally, the reduced density of states at $k_t = 0$ is 40% larger for the CB2-HH2 than CB1-HH1. At higher levels of carrier densities, the model predicts that maximum gain should occur at 1.57 μm, though we have yet to observe this experimentally.

Figure 4 shows the confinement factor of the optical field in the cladding, Γ_{clad}, region along with this factor in the quantum well region, Γ_{QW}. For our structure, $\Gamma_{QW} = 0.0139$. Such a small Γ_{QW} is the legacy of the broadened waveguide design. However, it is an agreeable tradeoff since by reducing Γ_{clad} to about 10%, the internal losses, measured below, fall to 2.5 cm^{-1}.

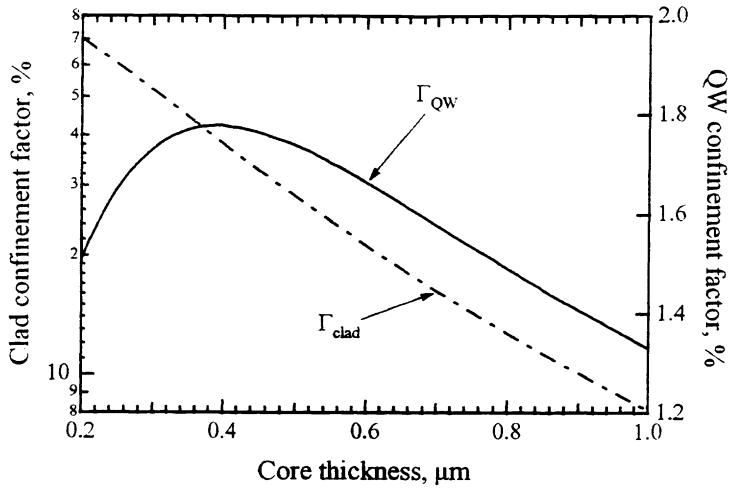

Figure 4. Confinement factor for the cladding region, Γ_{clad} and well, Γ_{QW} as a function of the core width. Though the optimum value of Γ_{QW} is 0.4 μm, the large coupling between the optical field and cladding leads to large internal losses. Devices presented here have a core thickness of 0.922 μm.

4. LASER CHARACTERIZATION

Initial tests focused on the relation between the GaSb substrate and the active material. 625 μm 4-QW devices were cleaved such that the laser axis of some bars was oriented in the [011] plane, while others were aligned perpendicular to this direction in the [0$\bar{1}$1]. This process was conducted to study the dependence of the cleaved-mirror quality, and thus the threshold current density, J_{th}, on the crystal orientation. The results are significant. Lasers aligned in the [0$\bar{1}$1] had an average J_{th} of 468 A/cm^2, but those oriented in the [011] averaged 389 A/cm^2. This difference is attributed to our empirical observation that the [011] and [0$\bar{1}\bar{1}$] planes of commercial GaSb substrates tend to cleave more smoothly. Subsequent lasers were cleaved along the optimum crystal plane and were tested for spectral qualities, lasing threshold, power, and efficiency.

The pulsed threshold current density, J_{th}, as function of the threshold gain, $g_{th} = \alpha_i - (1/2L)\ln(R_1R_2)$ (where R_1 and R_2 are the reflectivities of the mirrors, L is the cavity length, and α_i is the internal loss) is shown in Fig. 5. For these uncoated, cleaved-cavity devices, $R_1 \approx R_2 = 0.32$ and an internal loss of 2 cm^{-1} are assumed. All lasers are operating out of the first conduction sub-band to the first heavy-hole sub-band transition with wavelengths varying from 1.988 μm for the longest cavity lengths to 1.960 μm for the shortest. From Fig. 5, it is evident that the modal gain saturates at 61 cm^{-1} for the 2-QW and 75 cm^{-1} for the 4-QW. Although the saturated modal gain/QW for the 2-QW agrees well with theoretical calculations and is 50% greater than the saturated g_{mod}/QW reported by Garbuzov for similar lasers,[3] the data for the 4-QW structure is far below the expected value of 120 cm^{-1}. Our 2-QW result indicates that the 40% Al in the AlGaAsSb barrier gives better hole confinement, while the Garbuzov data for a GaInAsSb QW with 25% Al in the AlGaAsSb barrier suggests an optical transition in a bulk strained layer. This bulk gain effect may be occurring because either the valence band offset in the well is shallower than is commonly believed or the QW interfaces are unintentionally graded. In the case of the latter, a higher Al percentage in barrier would help confine carriers better at high bias. Since the x-ray diffraction data of Fig. 1 shows no evidence of strain relaxation in the 4-QW structure, it is believed that the trend in 4-QW threshold current density data results from uneven pumping of the wells. Because of the wide SCH layer and a smaller valence band energy discontinuity, holes injected over the energy barrier at the $Al_{0.9}Ga_{0.1}As_{0.07}Sb_{0.93}$ – $Al_{0.4}Ga_{0.6}As_{0.03}Sb_{0.97}$ (clad-core) heterojunction relax to the valence band edge of the $Al_{0.4}Ga_{0.6}As_{0.03}Sb_{0.97}$ barrier before reaching the QW region; consequently, the injection efficiency into the wells closer to the p-type $Al_{0.9}Ga_{0.1}As_{0.07}Sb_{0.93}$ is greater. Assuming quasi charge neutrality, a slower energy relaxation rate due to a smaller density of states, and a large conduction band offset, the electrons are more likely to overshoot the QW's and follow the holes within the SCH. Thus, the electrons are not preferentially captured in the wells closer to the n-type $Al_{0.9}Ga_{0.1}As_{0.07}Sb_{0.93}$ cladding layer. At the high carrier

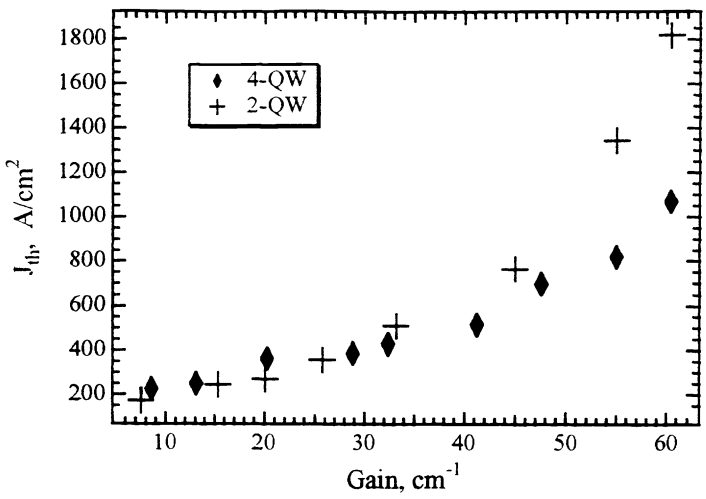

Figure 5. Measured threshold current density of 2 and 4-QW GaInAsSb/AlGaAsSb laser diodes as a function of the threshold gain in the Fabry-Perot cavity.

densities needed to saturate QW gain, hot phonons and degeneracy can reduce the energy relaxation rate by a factor of ten.[18] This has a much more pronounced effect on the electron distribution across the SCH because of the large amount of the energy that must be relaxed. It is not surprising, therefore, that near transparency, the low carrier density that is afforded in a strained quantum well laser means that the electrons and holes arrive at the QW region at the top of their respective bands. In this instance, the quasi-charge neutrality approximation dictates a more uniform carrier density distribution.

By extrapolating the data in Fig. 5 to zero threshold gain, the transparency current densities, J_0, of the 2- and 4-QW lasers are found to be 166 A/cm^2 and 216 A/cm^2, respectively. Assuming uniform pumping and that J_0 scales with the well number, a simple expression for J_o is obtained, viz., $J_o = J_{nr}$ + (J_o/ well) * well number. J_o/well is the sum of the radiative current density/well and the component of the non-radiative current density that scales with well number. A J_o/well of 25 A/cm^2 is calculated from the 2- and 4-QW $Ga_{0.81}In_{0.19}As_{0.03}Sb_{0.97}/Al_{0.4}Ga_{0.6}As_{0.03}Sb_{0.97}$ data. J_{nr} represents the component of the non-radiative current density that does not scale with well number. A value of 116 A/cm^2 is determined from the measured data for J_{nr}. Any contribution to the non-radiative current density from Auger recombination is expected to be contained within the J_o/well term since the Auger recombination scales with well number and is most likely to occur in the quantum well material. The radiative current density per well at transparency, J_{orad}/well, is calculated to be 10 A/cm^2. Consequently, the Auger component is no larger than 15 A/cm^2, and the current leakage over the valence band heterojunction is the dominant non-radiative contribution near transparency. Using the J_{th} data published by Garbuzov[7] for laser diodes with the same composition GaInAsSb well and AlGaAsSb clad layer but a smaller bandgap AlGaAsSb barrier layer, it is found that J_o/well = 20 $A/cm^2$and J_{nr} = 95 A/cm^2 for $Al_{0.25}Ga_{0.75}As_{0.02}Sb_{0.98}$ barrier material. Comparing this data to that presented in this work for $Al_{0.4}Ga_{0.6}As_{0.03}Sb_{0.97}$ barriers, it is observed that the J_o/well's and J_{nr}/ are similar.

For the 2-QW laser, the experimental measurements, shown in Fig. 5 can be modelled using the theoretical radiative current component, J_r, described in Sect. 3, plus an additional nonradiative component, J_{nr}. J_{nr} is attributed to interface recombination at the well-barrier interface and is given by $J_{nr} = \nu e d N_{well}/\tau_{nr}$ where ν is the number of wells and d the well width. A very good fit is obtained for τ_{nr} = 2.5 ns. In this case, an interface recombination velocity, v, given by d/τ_{nr} gives v = 376 cm/s. The 2-QW experimental measurements, reproduced from Fig. 5, along with the model result is shown in Fig. 6. This successful fitting tends to preclude any appreciable nonradiative component due to Auger recombination, at least for this temperature. Since the Auger current goes as N^3_{well}, J_{auger} increases extremely rapidly and does not fit well with the experimental data. However, investigations are still under progress.

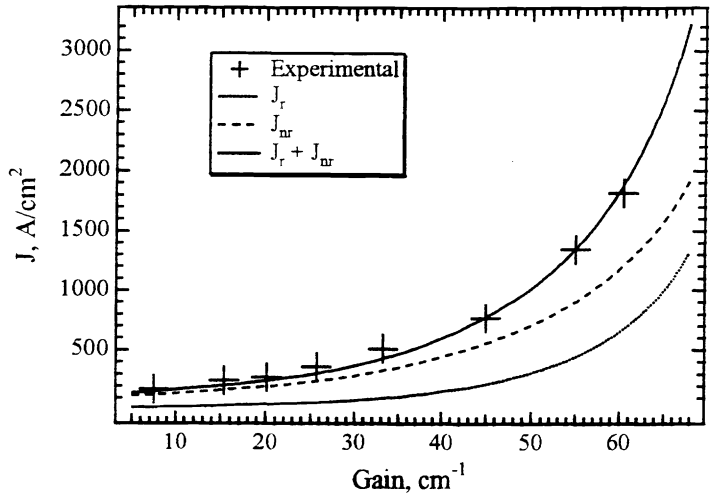

Figure 6. The 2-QW J_{th} versus the threshold gain (crosses) is plotted along with the model, J_{tot}. $J_{tot} = J_r + J_{nr}$ where J_r (dotted line) is the radiative component calculated in Sect. 3 and J_{nr} (dashed line) is a recombination term linearly proportional to the well carrier density.

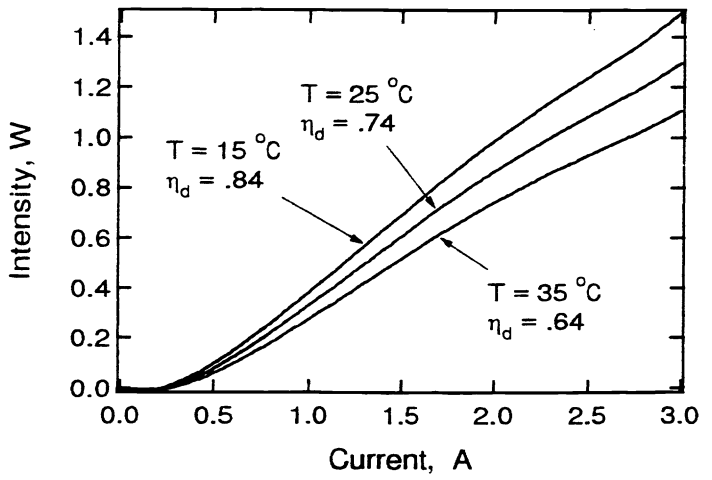

Figure 7. Total power emitted from both facets of a 900 μm 2-QW laser at various temperatures. At 15 °C, the differential efficiency, $\eta_d = 0.84$.

The total output power curves of the best 900 μm 2-QW laser are shown in Fig. 7 for temperatures of 15 °C, 25 °C, and 35 °C. The laser, impedance matched with the current source, is operating in a pulsed mode with a 100 ns pulse width and a 100 kHz repetition rate (1% duty cycle). Threshold current densities, J_{th}, are 187 A/cm^2, 208 A/cm^2, and 228 A/cm^2 respectively and the differential efficiencies, η_d, are .84, .74, and .64. For this particular device, the characteristic temperature, T_0, is 101 °K.

The internal efficiency, η_i, and internal loss, α_i , are determined by plotting η_d^{-1} versus the cavity length L, then fitting to a line using $\eta_d^{-1} = \eta_i^{-1}(1 - \alpha_i L/\ln R)$. Results obtained from averaging η_d obtained from all the light-current curves of 2-QW lasers for 5 different cavity lengths are shown in Fig. 8. This data was taken at a

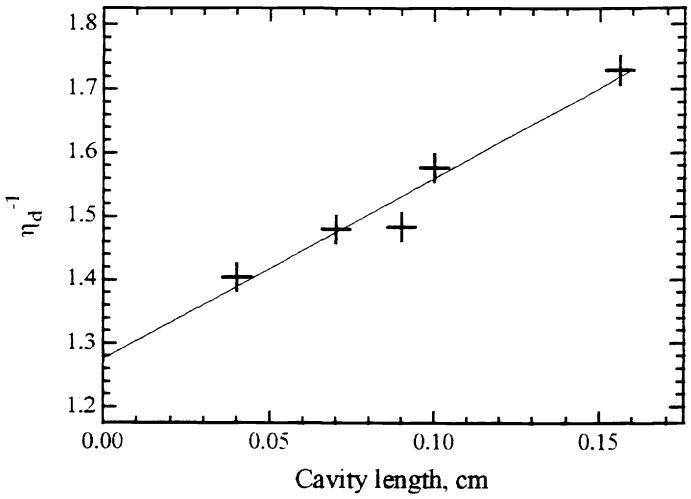

Figure 8. The inverse differential efficiency, η_d^{-1}, is plotted versus the laser cavity length. The internal efficiency, η_i, and losses, α_i, are derived from a linear curve fit of the experimental data points (crosses).

temperature of 25 °C. A line fit to the data yields η_i, = 0.8 and α_i = 2.5 cm^{-1}.

In comparison with the broadest waveguide laser of Ref. 3, our measurement of α_i is comparable to their measured value of 2 cm^{-1} In contrast, our measured η_i is substantially larger (0.8 to 0.6). This superiority stems from the greater barrier potential imposed by the 40% Al barrier. The thermionic emission time of carriers from the well,τ_e, increases exponentially with the barrier and thus has a dramatic effect. The transport factor, $\chi = (1 + \tau_r/\tau_e)$ will be reduced and η_i will be increased since the probability of recombination by stimulated emission is enhanced at the expense of barrier recombination processes.[19]

Finally, the temperature sensitivity of the devices is investigated. The spectrum of the tested lasers ranged from 1.960 μm to 1.988 μm and, naturally, is a function of the device and temperature. Spectral qualities of the individual lasers varied with the best 2-QW laser having a sharp single peak at 1.972 μm at T = 18 °C. At 35 °C, this laser operated at 1.990 μm which is a shift 1.06 nm/ °C. Figure 9 is a log-linear plot of the lasing threshold current as a function of temperature for the 1025 μm 4 QW laser. Data is obtained using a computer controlled procedure from T= 14 °C up to T= 72 °C with a step size of approximately 1.5 °C. The threshold current is designated to occur at the maximum change in slope of the light-current curve. Using $I = I_o e^{T_0/T}$, where T_0 is the characteristic temperature, a line fit to the data in Fig. 9 produces two dominant values of T_0. For T < 50 °C, T_0 = 140 °K. This is the largest reported T_0 to date for a semiconductor laser with $\lambda \geq 1.3\mu$m. This high value of T_0 tends to support the use of the high Al content in the AlGaAsSb barrier. This higher potential traps the electrons in the wells and minimizes carrier spillage that would otherwise lead to lower values of T_0. Furthermore, for typical operating temperatures, little evidence of an Auger recombination current component is displayed. For this laser, J_{th} = 248 A/cm^2. As in the 2-QW case, J_{th} per-well = 25 A/cm^2 and thus the leakage current is 148 A/cm^2. Above 50 °C, however, the characteristic temperature decreases to 74 °K. It is probable that for higher temperatures, Auger processes begin to play a role.

5. SUMMARY AND DISCUSSION

Previous research has shown that 2 μm GaInAsSb/AlGaAsSb quantum well (QW) laser diodes demonstrate low threshold current density and acceptable slope efficiency. However, optimal material design parameters have not been identified, especially as regards the valence band offset in the QW. The optical characteristics of multiple QW lasers with $Ga_{.81}In_{.19}As_{.02}Sb_{.98}$ wells and $Al_{0.4}Ga_{0.6}As_{0.03}Sb_{0.97}$ barriers lasers grown by molecular beam epitaxy (MBE) have been presented. The lowest measured threshold current densities for 2- and 4-QW devices are 173 and 226 A/cm^2, respectively, which are among the lowest reported values to date. The valence band offset for these

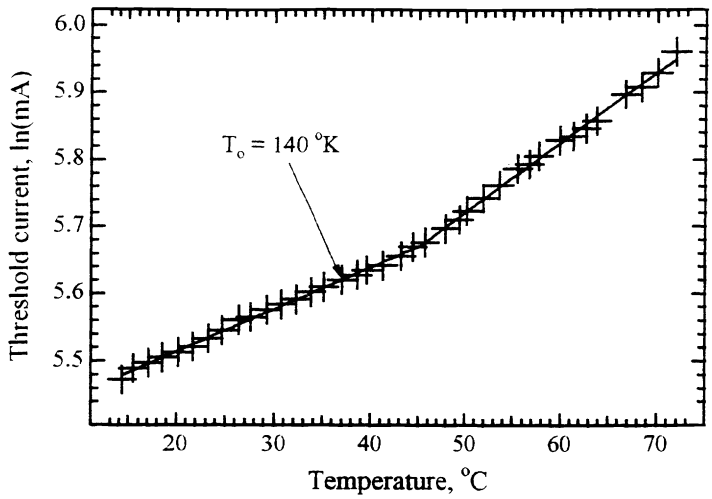

Figure 9. A log-linear plot of I_{th} versus T for the 1025 μm 4 QW laser. The 140 °K characteristic temperature is the highest yet reported for semiconductor lasers operating above 1.3 μm.

lasers is larger than has previously been studied and leads to better hole confinement. The benefit of a larger ΔE_v is demonstrated by a 50% higher saturated modal gain/well measured for 2-QW lasers and a record characteristic temperature, T_0 = 140 °K, measured for a 1 mm cavity length, 4-QW device (see Fig. 9). This is the highest T_0 reported to date for either antimonide or phosphide based lasers at 2 μm. From theoretical computations and their comparison with experimental data, it is found that parasitic leakage current dominates near optical transparency and that Auger recombination contributes little to the non-radiative current.

Two issues are presently being studied in this system. First, the performance on a per-well basis of the 4-QW devices is not substantially superior to the 2-QW versions. An x-ray diffractometry profile of the asymmetric [115] plane and the symmetric [004] plane scans preclude the possibility of strain relaxation in the 4-QW structure. Hence it is feasible that the wells are unevenly pumped at high current levels due to a greater injection efficiency of the holes into wells nearby the p-type cladding barrier. Second, initial modeling indicates that the nonradiative current contribution to J is linearly proportional to the well carrier density, see Fig. 6. In such a case, J_{nr} would scale with the number of wells. However, we have not observed this to date. The reason is attributed to leakage currents in the diode laser. This process will produce a component to J_{nr} that is constant. Consequently, the origin of the nonradiative current have yet to be entirely resolved. These two issues are being investigated.

Finally, it is interesting to note that a substantial increase in the lasing threshold will occur in this material if left uncoated. When 425 μm 4-QW lasers were first cleaved, the average J_{th} was found to be 203 mA. Though predominantly stored in a nitrogen chamber, several months later J_{th} had increased to 300 mA due to degradation of the facet surfaces. With the approximation $g = g_o \ln(J/J_{tr})$ where g is the gain, along with $g = \alpha_i + \alpha_m$, then the consequence of continuous exposure to the environment is a reduction in the effective mirror reflectivity from 32% to 23.5%. Nevertheless, this does not detract from the exceptional performance of the GaInAsSb/AlGaAsSb QW laser.

6. ACKNOWLEDGMENTS

This work was supported by AFOSR under grant F49620-96-1-0079 and the Army Federated Laboratories. The views and conclusions contained in this document are those of the authors and should not be interpreted as representing the official policies, either expressed or implied, of the Army Research Laboratory or the U.S. Government.

REFERENCES

1. H. Lee, P. K. York, R. J. Menna, R. U. Martinelli, D. Z. Garbuzov, S. Y. Narayan, and J. C. Connolly, "Room temperature 2.78 μm AlGaAsSb/InGaAsSb quantum-well lasers," *Appl. Phys. Lett.* **66**, pp. 1942–1944, 1995.

2. D. Z. Garbuzov, R. U. Martinelli, R. J. Menna, P. K. York, H. Lee, S. Y. Narayan, and J. C. Connolly, "2.7-μm InGaAsSb/AlGaAsSb laser diodes with contiuous-wave operation up to -39 °C," *Appl. Phys. Lett.* **67**, pp. 1346–1348, 1995.
3. D. Z. Garbuzov, R. U. Martinelli, H. Lee, P. K. York, R. J. Menna, J. C. Connolly, and S. Y. Narayan, "Ultra-low loss broadened waveguide high-power 2 mm AlGaAsSb/InGaAsSb/GaSb separate-confinement quantum-well lasers," *Appl. Phys. Lett.* **69**, pp. 2006–2008, 1996.
4. H. K. Choi, G. W. Turner, and S. J. Eglash, "High-power GaInAsSb-AlGaAsSb multiple-quantum-well diode-lasers emitting at 1.9-μm," *IEEE Photon. Tech. Lett.* **6**, pp. 7–9, 1994.
5. H. K. Choi, G. W. Turner, M. K. Connors, S. Fox, C. Dauga, and M. Dagenais, "High-power, high-temperature operation of GaInAsSb-AlGaAsSb ridge-wave-guide lasers emitting at 1.9-μm," *IEEE Photon. Tech. Lett.* **7**, pp. 281–283, 1995.
6. W. Z. Shen, Y. Chang, S. C. Shen, W. G. Tang, Y. Zhao, and A. Z. Li, "Temperature-dependent exciton behavior in quaternary GaInAsSb/AlGaAsSb strained single quantum-wells," *J. Appl. Phys.* **79**, pp. 2139–2141, 1996.
7. D. Z. Garbuzov, R. U. Martinelli, H. Lee, R. J. Menna, P. K. York, L. A. DiMarco, M. G. Harvey, R. J. Matarese, S. Y. Narayan, and J. C. Connolly, "4 W quasi-continuous-wave output power from 2 mm AlGaAsSb/InGaAsSb single-quantum-well broadened waveguide laser diodes," *Appl. Phys. Lett.* **70**, pp. 2931–2933, 1997.
8. J. C. DeWinter, M. A. Pollack, A. K. Srivastava, and J. L. Zyskind, "Liquid-phase epitaxial Ga1-xInxAsySb1-y lattice-matched to (100) GaSb over the 1.71-μm 2.33-μm wavelength range," *J. Electron. Mater.* **14**, pp. 729–747, 1985.
9. Landolt and Bornstein in *Numerical Data and Functional Relationships in Science and Technology, vols 17a and 17b*, O. M. M. Shultz and H. Weiss, eds., Springer, New York, 1982.
10. Y. Tsou, A. Ichii, and E. M. Garmire, "Improving InAs double heterostructure lasers with better confinement," *J. Quantum Elect.* **28**, p. 1261, 1992.
11. B. Batterman, , and G. Hildebrandt *Acta Cryst. A* **24**, pp. 150–157, 1968.
12. A. Krost, J. Bohrer, A. Dadger, R. F. Schnabel, D. Bimberg, S. Hansmann, and H. Burkhard, "High-resolution x-ray-analysis of compressively strained 1.55 μm GaInAs/AlGaInAs multiquantum-well structures near the critical thickness," *Appl. Phys. Lett.* **67**, pp. 3325–3327, 1995.
13. P. Y. Yu and M. Cardona, *Fundamentals of Semiconductors*, Springer-Verlag, New York, 1996.
14. J. M. Luttinger and W. Kohn, "Motion of electrons and holes in perturbed periodic fields," *Phys. Rev.* **97**, pp. 869–883, 1955.
15. D. A. Broido and L. J. Sham, "Effective masses of holes at GaAs-AlGaAs heterojunctions," *Phys. Rev. B.* **31**, pp. 888–892, 1985.
16. S. Corzine, R.-H. Yan, and L. A. Coldren, "Optical gain in iii-v bulk and quantum well semiconductors," in *Quantum Well Lasers*, P. Zory, ed., pp. 17–96, Academic Press, Boston, 1993.
17. M. Altarelli, U. Ekenberg, and A. Fasolino, "Calculations of hole subbands in semiconductor quantum wells and superlattices," *Phys. Rev. B.* **32**, pp. 5138–5143, 1985.
18. L. F. Lester and B. K. Ridley, "Hot carriers and the frequency-response of quantum-well lasers," *J. Appl. Phys.* **72**, pp. 2579–2588, 1992.
19. R. Nagarajan, R. P. Mirin, T. E. Reynolds, and J. E. Bowers, "Effect of the confinement-layer composition on the internal quantum efficiency and modulation response of quantum-well lasers," *IEEE Phot. Tech. Lett.* **4**, pp. 832–834, 1992.